Crystal Structure of an Electron Transfer Complex between Aromatic Amine Dehydrogenase and Azurin from *Alcaligenes faecalis*[†,‡]

Narayanasami Sukumar,[§,||] Zhi-wei Chen,[§] Davide Ferrari,[⊥] Angelo Merli,[⊥] Gian Luigi Rossi,[⊥] Henry D. Bellamy,[@,+] Andrei Chistoserdov,[#] Victor L. Davidson,[●] and F. Scott Mathews*[,§]

Department of Biochemistry and Molecular Biophysics, Washington University School of Medicine, St. Louis, Missouri 65211, Department of Biochemistry and Molecular Biology, University of Parma, Parma, Italy, Stanford Synchrotron Radiation Laboratory, Stanford, California 94309, Department of Biology, University of Louisiana, Lafayette, Louisiana 70504, and Department of Biochemistry, University of Mississippi Medical Center, Jackson, Mississippi 39216

Received June 28, 2006; Revised Manuscript Received September 6, 2006

ABSTRACT: The crystal structure of an electron transfer complex of aromatic amine dehydrogenase (AADH) and azurin is presented. Electrons are transferred from the tryptophan tryptophylquinone (TTQ) cofactor of AADH to the type I copper of the cupredoxin azurin. This structure is compared with the complex of the TTQ-containing methylamine dehydrogenase (MADH) and the cupredoxin amicyanin. Despite significant similarities between the two quinoproteins and the two cupredoxins, each is specific for its respective partner and the ionic strength dependence and magnitude of the binding constant for each complex are quite different. The AADH−azurin interface is largely hydrophobic, covering ∼500 Å^2 of surface on each molecule, with one direct hydrogen bond linking them. The closest distance from TTQ to copper is 12.6 Å compared with a distance of 9.3 Å in the MADH−amicyanin complex. When the MADH−amicyanin complex is aligned with the AADH−azurin complex, the amicyanin lies on top of the azurin but is oriented quite differently. Although the copper atoms differ in position by ∼4.7 Å, the amicyanin bound to MADH appears to be rotated ∼90° from its aligned position with azurin. Comparison of the structures of the two complexes identifies features of the interface that dictate the specificity of the protein−protein interaction and determine the rate of interprotein electron transfer.

Specific interaction between proteins whose physiological function involves transfer of electrons from one to another is critical for the proper orientation of the donor and acceptor redox centers and for preventing misdirected electron flow which would waste energy and potentially damage cell components. This is particularly true for soluble redox proteins which tend to be weakly associating when they interact. While crystal structures are available for several redox proteins, there are relatively few cases in which a complex of two or more soluble natural redox protein partners has been crystallized and structurally characterized. These include complexes between cytochrome *c* and cytochrome *c* peroxidase (*1*), cytochrome *c* and the yeast cytochrome bc_1 complex (*2*), electron transfer flavoprotein (ETF) and medium chain acyl CoA dehydrogenase (*3*), ETF and trimethylamine dehydrogenase (*4*), ferredoxin and ferredoxin-NADP$^+$ reductase (*5*), methylamine dehydrogenase (MADH)[1] and amicyanin (*6*), and a ternary complex of the latter with cytochrome c_{551i} (*7*). Such structural information is important for understanding the features which dictate the specificity of the protein−protein interaction and elucidating mechanisms of interprotein ET. We report here the crystal structure of the complex of the quinoprotein aromatic amine dehydrogenase (AADH) with its likely natural ET acceptor protein, azurin.

AADH from *Alcaligenes faecalis* catalyzes the oxidative deamination of aromatic amines, including tyramine and dopamine (*8*, *9*). It is an $\alpha_2\beta_2$ heterotetramer with subunit molecular masses of 39 and 18 kDa, respectively, and is located in the periplasm. AADH contains tryptophan tryptophylquinone (TTQ) (*10*) as its redox cofactor. Transient kinetic studies of the reductive half-reaction using tyramine as substrate and an artificial electron acceptor (phenazine methosulfate) show a large primary deuterium kinetic isotope effect (*11*); abstraction of a proton from the Cα atom appears to be rate-limiting. It has recently been shown that the reaction chemistry of the reductive half-reaction of AADH is dominated by proton tunneling (*12*).

When *A. faecalis* cells are grown on β-phenethylamine, a condition under which AADH is induced, large amounts of

[†] This work was supported by NSF Grant MCB-0343374 (F.S.M.), NIH Grant GM41574 (V.L.D.), and PRIN 2005050270_002 (G.L.R.).

[‡] Crystallographic coordinates have been deposited in the Protein Data Bank as entries 2H47, 2IAA, and 2H3X for crystal forms 1−3, respectively, of the AADH−azurin complex.

* To whom correspondence should be addressed. Telephone: (314) 362-1080. Fax: (314) 362-7183. E-mail: mathews@biochem.wustl.edu.

[§] Washington University School of Medicine.

[||] Present address: NE-CAT, Sector 24, Building 436E, Argonne National Laboratory, Argonne, IL 60439.

[⊥] University of Parma.

[@] Stanford Synchrotron Radiation Laboratory.

[+] Present address: Center for Advanced Microstructures and Devices, 6980 Jefferson Highway, Baton Rouge, LA 70806.

[#] University of Louisiana.

[●] University of Mississippi Medical Center.

[1] Abbreviations: AADH, aromatic amine dehydrogenase; MADH, methylamine dehydrogenase; PSCAM, polarized single-crystal absorption microspectrophotometer; rmsd, root-mean-square deviation.

10.1021/bi0612972 CCC: $33.50
Published on Web 10/24/2006

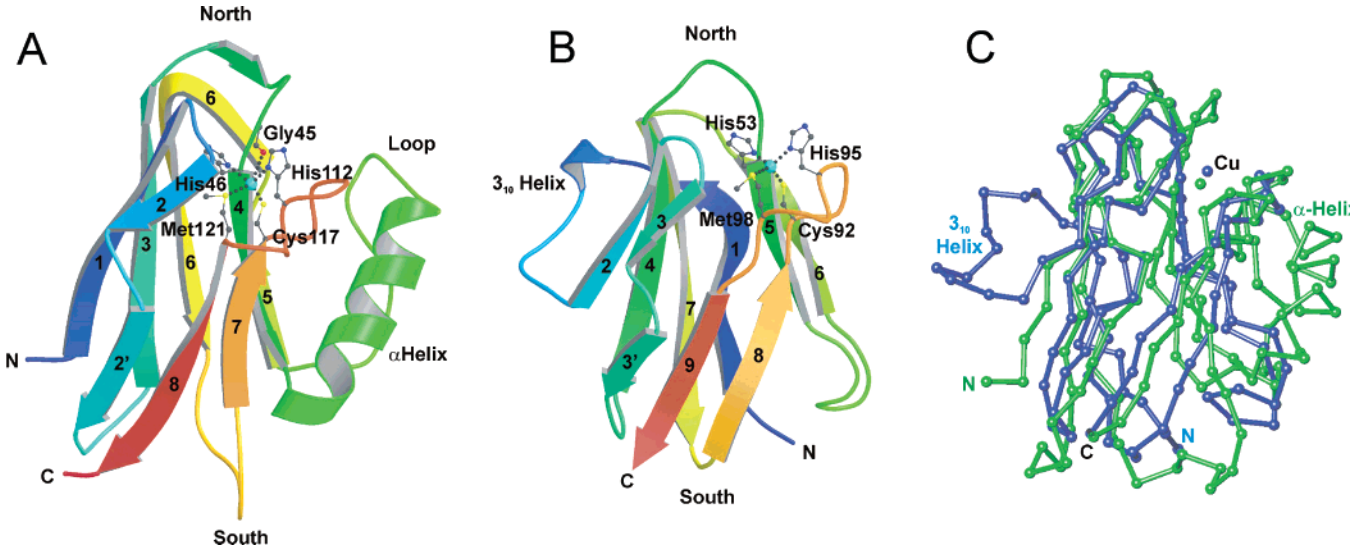

FIGURE 1: Structural diagrams of azurin and amicyanin. (A) Ribbon diagram of azurin from *A. denitrificans*. The rainbow color of the molecule progresses from the N-terminus in blue to the C-terminus in red. The five copper ligands, shown as ball-and-stick diagrams, are labeled along with the N- and C-termini; the β-strands are numbered sequentially from 1 to 9, and the loop and helix between strands 4 and 5 are also labeled. The so-called "north" and "south" ends of the molecule are indicated. (B) Ribbon diagram of amicyanin from *P. denitrificans*. The coloring and labeling are similar to those in panel A. (C) Cα diagram of azurin (green) superimposed on amicyanin (blue). Panels A and B were prepared using Molscript (*39*) and Raster3D (*40*); panel C was prepared using Turbo-Frodo (*31*).

azurin are also produced (*13*). In vitro, azurin can act as a good acceptor of electrons from AADH. Steady state oxidation of AADH by azurin follows Michaelis−Menten kinetics with a k_{cat} of 64 s^{-1} and a K_M of 137 μM at 30 °C in low salt [0.01 M potassium phosphate (pH 7.5)]; in high salt (0.25 M buffer), k_{cat} = 91 s^{-1} and K_M = 44 μM (*14*). Transient kinetic studies of the electron transfer reaction from AADH to azurin were performed together with solvent kinetic isotope effects and analysis of the temperature dependence of the limiting first-order rate constants. The results indicated that the reaction of the hydroquinol TTQ that is generated by reduction of AADH by dithionite was a true electron transfer reaction, whereas the reaction of the aminoquinol TTQ that is generated by reduction of AADH by the amine substrate was gated by a proton transfer step that is rate-limiting for electron transfer (*15*). In the latter, the proton transfer activates the system so that the gated reaction is actually much faster for the aminoquinol than the true electron transfer reaction for the hydroquinol. This is an example of chemically gated electron transfer (*16*). Since the reaction of the hydroquinol is rate-limited by the electron transfer event, it was possible to determine values for electron parameters, reorganization energy and electronic coupling, that are associated with the electron transfer and to experimentally predict the electron transfer distance. It is now possible to evaluate these previous results in the context of the structure of the electron transfer protein complex presented here.

AADH is ~30% identical in sequence to another bacterial quinoprotein, the TTQ-containing MADH from *Paracoccus denitrificans* (*17*). Many of the kinetic and structural properties of AADH and MADH are very similar (*14*). MADH is an $\alpha_2\beta_2$ heterotetramer with subunit molecular masses of 45 and 15 kDa respectively. Its electron acceptor in vivo is amicyanin, a small cupredoxin similar to azurin. The transient kinetic behavior for the reductive half-reaction of MADH using methylamine as a substrate and phenazine methosulfate as an electron acceptor is similar to that observed with AADH (*18*). The transient kinetic behavior of the oxidative half-reaction with respect to the aminoquinol or hydroquinol forms of reduced TTQ is also similar between the two enzymes, with proton transfer limiting the former rate and electron transfer limiting the latter rate.

However, there are also a number of significant differences between the two enzymes. They are not immunologically cross reactive (*8*). Furthermore, the substrate specificity of AADH is quite different from that of MADH, with large aromatic and hydrophobic substrates being preferred by the former and small aliphatic substrates by the latter. The electron acceptors are also different and highly specific. Azurin is not an effective electron acceptor for MADH, and amicyanin is not an effective electron acceptor for AADH (*14*). Furthermore, amicyanin binds much more tightly to MADH than azurin does to AADH, with K_d values, determined by ultrafiltration at low ionic strengths, of 4.5 and 300 μM, respectively (*14*, *19*). The ionic strength dependence of the stability of the two complexes also differs. For AADH, the steady state value of K_M for reoxidation by azurin drops 3-fold upon going from 0.01 to 0.25 M phosphate buffer (*14*), while for MADH, the steady state value of K_M for reoxidation by amicyanin increases 8-fold upon the addition of 0.2 M sodium chloride (*20*).

Azurin and amicyanin are both type I blue copper proteins, with molecular masses of 15 and 12.5 kDa, respectively, that function as soluble electron carriers (*21*, *22*). They are both cylindrically shaped molecules that form β-sandwich structures made up of eight and nine antiparallel β-strands, respectively (Figure 1). Strand 1 and a connecting 3/10-helical loop of amicyanin are absent in azurin, and azurin contains a short helix−loop motif inserted between β-strands 4 and 5 of the β-sandwich that is absent from the analogous location of amicyanin. Central cores of 61 spatially equivalent Cα atoms common to azurin and amicyanin, which are 21% identical in sequence, align with a root-mean-square deviation (rmsd) of 1.78 Å, leaving the copper atoms 1.3 Å apart (Figure 1). In both proteins, the copper is bound by

Table 1: Crystal Data, Data Collection, and Refinement Statistics for the AADH−Azurin Complex

	crystal form 1	crystal form 2	crystal form 3
Crystal Data			
crystal system		orthorhombic	
space group		$P2_12_12_1$	
unit cell parameters (Å)			
a	97.5	67.2	64.9
b	124.6	131.7	94.8
c	189.9	133.2	211.5
Data Collection			
X-ray source	Rigaku RU200	APS SBC-19ID	APS NE-CAT-8BM
wavelength (Å)[a]	1.5418	1.381/1.445	1.375
resolution range (Å) (last shell)	40−2.6 (2.69−2.60)	40−1.95 (2.02−1.95)	40−2.5 (2.59−2.50)
no. of unique reflections	50339	80177	34130
redundancy	3.4	5.5	4.3
completeness (last shell) (%)[b]	69.2 (39.2)	92.8 (69.7)	74.4 (62.4)
R_{merge} (last shell)[c]	0.058 (0.118)	0.103 (0.202)	0.096 (0.460)
$I/\sigma(I)$[d] (last shell)	17.8 (5.9)	14.2 (3.4)	13.1 (2.4)
Refinement			
resolution range (Å)	40−2.6	40−1.95	40−2.5
R-factor (%)[e,f]	0.188	0.174 (0.162)	0.183
R_{free} (%)[e,g]	0.249	0.205 (0.184)	0.230
model			
no. of amino acids	2072	1072	1223
no. of waters	747	989	651
average *B*-factor for chain α (Å^2)	23.7	21.9	27.7
average *B*-factor for chain *β* (Å^2)	31.5	21.9	29.7
average *B*-factor for chain AZU (Å^2)	68.3	63.5	61.2
average *B*-factor of solvent atoms (Å^2)	25.1	35.8	34.2
residues in generously allowed regions (%)	0.5	0.2	0.3
residues in disallowed region (%)	0.5	0.4	0.5
stereochemical ideality			
bonds (Å)	0.006	0.005	0.006
angles (deg)	1.51	1.44	1.42
dihedral angles (deg)	25.8	25.8	25.9
improper angles (deg)	0.89	0.79	0.80

[a] The data for crystal form 2 were recorded at two wavelengths and were combined to improve their redundancy and completeness. Since the lower-energy data set was limited to 2.1 Å resolution, the redundancy and completeness drop sharply in the 2.1−1.95 Å resolution range as indicated in the table. When analyzed in the more limited resolution range of 40−2.1 Å, the overall completeness for the combined data set is 96.7% and for the outer shell (2.18−2.10 Å resolution) is 92.1%. [b] The completeness of data sets 1 and 3 was low because of overlap of the reflection data caused by the long *c*-axis and by high crystal mosaicity. [c] $R_{merge} = \sum|I_i - I|/\sum I_i$, where I_i is the intensity of the *i*th observation, *I* is the mean intensity of the reflection, and the summation extends over all data. [d] $I/\sigma(I)$ is the average signal-to-noise ratio for merged reflection intensities. [e] *R*-factor = $\sum||F_o| - |F_c||/\sum|F_o|$, where $|F_o|$ is the observed structure factor amplitude, $|F_c|$ is the calculated structure factor amplitude, and the summation extends over all data. [f] The values in parentheses are the results obtained after two cycles of TLS refinement in REFMAC, as described in the text. [g] R_{free} is the *R*-factor obtained for a test set of reflections, consisting of a randomly selected 10% subset of the diffraction data, not used during refinement.

four protein side chain ligands, two histidines, one cysteine, and one methionine. In azurin, the copper is also coordinated by a fifth ligand, donated by a main chain carbonyl oxygen atom.

In this paper, we report the structure of the AADH−azurin complex as determined from three different crystal forms and compare its structure to that of the MADH−amicyanin complex (*7*). Polarized single-crystal absorption microspectrophotometry (*23*, *24*) is used to demonstrate that the protein complex is competent for catalysis and interprotein electron transfer in the crystalline state. The new structure also allows interpretation of previous electron transfer studies in elucidating the structural basis for differences in the experimentally determined values for electronic coupling and electron transfer distance determined for the electron transfer reactions in the AADH−azurin and MADH−amicyanin complexes.

MATERIALS AND METHODS

Protein Purification. AADH and azurin were isolated and purified from *A. faecalis* as described previously (*8*, *13*).

Crystallization and Data Collection. Three crystal forms of the AADH−azurin complex were prepared by the sitting-drop vapor-diffusion method (*25*) by first mixing AADH and azurin, each dissolved in 10 mM K/Na phosphate buffer (pH 7.5) in a 1:1 molar ratio with respect to TTQ and copper and then concentrating the resulting solution to a protein concentration of 10 mg/mL. Sitting drops were then prepared by mixing 5 μL of protein solution with 5 μL of reservoir solution in a 24-well Cryschem plate (Hampton Research, Laguna Niguel, CA). The sitting drops were then equilibrated with 1 mL of reservoir solution at 20 °C after sealing the wells with clear sealing tape. Crystal form 1 was obtained from 23−28% PEG4000, 0.1 M Tris buffer (pH 8.5), and 0.2 M sodium acetate. Crystal form 2 was obtained from 20% PEG8000, 0.1 M Mes buffer (pH 6.0), and 0.15 M calcium acetate. Crystal form 3 was obtained from 29.5% PEG4000, 0.1 M Tris buffer (pH 8.5), and 0.1 M potassium acetate. All three crystal forms are orthorhombic, in space group $P2_12_12_1$. The unit cell dimensions are presented in Table 1. X-ray diffraction data from single crystals of each of all three crystal forms were collected at 100 K with 20% glycerol added to an artificial mother liquor appropriate to each form as a cryoprotectant. For crystal form 1, the data

were recorded in house with a Rigaku R-axis IV detector using Cu Kα radiation ($\lambda = 1.5418$ Å) from an RU200 X-ray generator operated at 5 kW power to a resolution of 2.6 Å. For crystal form 2, the data were recorded to 1.95 and 2.10 Å resolution at beamline 19ID of the Structural Biology Center (SBC) at the Advanced Photon Source (APS), Argonne IL. For these two data sets, the X-ray energy was tuned to the peak (f'') and to a low-energy remote point of the copper fluorescence spectrum. For crystal form 3, the data were recorded to 2.50 Å resolution at beamline 8BM of the NE-CAT of the APS, with the X-ray energy tuned at the peak of the copper fluorescence spectrum. The data from all three crystals were processed using HKL2000 (*26*), and for the purposes of refinement, the two data sets from crystal form 2 were merged, also using HKL2000, to improve the data redundancy and completeness. The data collection statistics are summarized in Table 1.

Polarized Single-Crystal Absorption Microspectrophotometry (PSCAM). The methodology of polarized absorption spectroscopy of oriented single crystals is well-established (*27*−*29*). The crystals were placed in a flow cell with quartz windows, and the aqueous surroundings of the crystal were varied by flowing fresh solutions of various pH containing a variety of salts, reducing or oxidizing agents, past the crystal. Spectra were recorded using plane-polarized light with the electric vector parallel to one of the principal optical directions or the other lying on the crystal face perpendicular to the incident beam. A Zeiss MPM800 microspectrophotometer was used.

Crystal Structure Analysis. The structures of all three crystal forms of the AADH−azurin complex were determined initially by molecular replacement in MOLREP (*30*) using the structure of AADH determined at 1.2 Å resolution (*12*) as a search model. In each case, the positions and orientations of one or two molecules of the $\alpha_2\beta_2$ AADH heterotetramer could be readily identified. Partial refinement of AADH by rigid body and positional refinement were carried out in CNS (*31*). For both AADH subunits, the residue numbering begins from the first translated methionine of the premature protein.

No structure of azurin from *A. faecalis* has been reported, although the amino acid sequence is available (R. P. Ambler, Swiss-Prot entry P00281). The position of a single copper ion in crystal form 2 of the complex was identified in an anomalous scattering (Bijvoet) difference map using symmetry-averaged values of $\langle F(hkl)\rangle - \langle F(-h,-k,-l)\rangle$ as Fourier coefficients obtained from the anomalous scattering data recorded at the SBC and the partial phase information obtained by molecular replacement. A model of azurin from *Alcaligenes denitrificans* (PDB entry 2AZA) (*21*) was then fit to difference maps computed using $|2F_o - F_c|$ as Fourier coefficients, where the structure factors (F_c) were calculated from the AADH models and the phases were obtained from the partial refinement. The azurin molecule was placed so that its copper position was centered at the anomalous peak obtained from the Bijvoet difference map and was rotated manually as a rigid body, using the molecular graphics package TURBO-FRODO (*32*), to match the difference electron density. Since the sequences of the *A. faecalis* and *A. denitrificans* azurin molecules are only 67% identical, the nonidentical side chains of the *A. denitrificans* sequence were changed to those of *A. faecalis* and their positions were adjusted where necessary. The model of azurin bound to AADH was then improved by alternate cycles of model building and refinement using CNS, and water molecules were gradually introduced into the model. A Bijvoet difference map was also computed for crystal form 3 using the NE-CAT data which indicated two copper sites. Both of these sites were then fit by the *A. faecalis* azurin molecule obtained from crystal form 2 and adjusted and refined in the same manner. Since the data for the form 1 crystal were collected in house with Cu Kα radiation, no anomalous signal could be detected. The single azurin binding site was identified by matching the AADH portion of the AADH−azurin model from crystal form 2 to each of the four AADH heterodimers in the asymmetric unit of form 1 and comparing the associated azurin model to the electron density. The single azurin model that correlated well with the calculated electron density was then adjusted and refined using CNS. After the last cycle of refinement of the crystal form 2 model in CNS, two cycles of refinement using REFMAC of the CCP4 package (*30*) were carried out. During the refinement, the model was divided into five groups, one for each polypeptide chain, for TLS refinement (*33*, *34*), and for modeling anisotropic displacement parameters. The final refinement statistics are listed in Table 1.

Electron transfer coupling analysis was performed using the HARLEM computer program (*35*) by the Pathways approach of Beratan, Onuchic, and co-workers (*36*).

Surface area calculations were carried out using AREAIMOL in the CCP4 computing suite (*30*). For structural comparisons with the AADH−azurin complex, coordinates for the MADH−amicyanin complex were taken from PDB entry 2GC4.

RESULTS

Verification and Determination of the Structure of the AADH−Azurin Complex. The first crystal of the AADH−azurin complex to be grown (form 1) did not display visually a distinctive blue coloration, unlike initial crystals of the MADH−amicyanin complex (*6*). Polyacrylamide gel electrophoresis of a single crystal of the putative complex revealed two bands at roughly 45 and 15 kDa, suggesting that azurin, if present, and the β-subunit of AADH were comigrating. An X-ray fluorescence spectrum (data not shown) of a cluster of small crystals recorded at the Stanford Synchrotron Radiation Laboratory exhibited a weak signal at the expected energy for copper but could have been caused by an impurity. However, polarized single-crystal absorption microspectrophotometry (PSCAM) spectra, recorded from a single crystal (form 1) along two perpendicular principal directions, showed the main absorption of oxidized TTQ (maximum at 456 nm in solution) and a broad band above 600 nm, attributable to both oxidized copper and oxidized TTQ. When the crystal was treated with sodium ascorbate, spectral changes occurred, as a consequence of redox reactions, and the magnitude of the high-wavelength band substantially decreased in one of the polarized spectra. The difference spectra (prior to and after treatment with ascorbate) exhibited distinct maxima and minima, in particular at 625 nm (the position characteristic of oxidized copper) and 330 nm (the position characteristic of reduced TTQ), suggesting that complete reduction of an azurin component and a partial

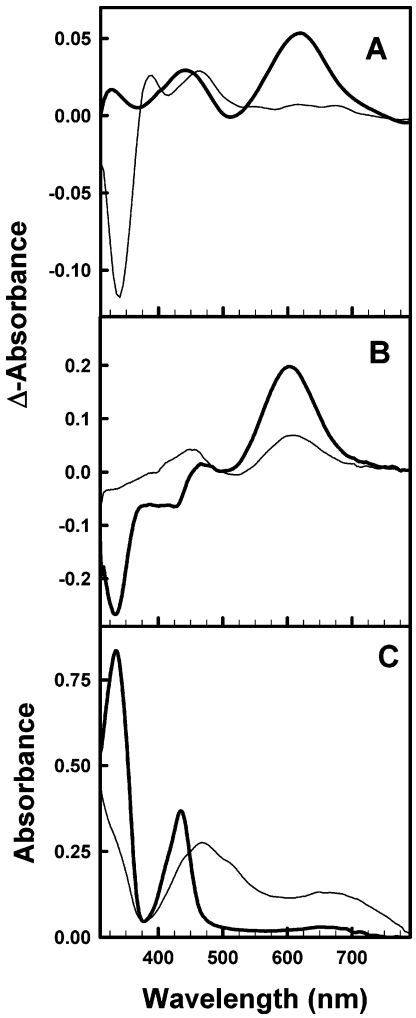

FIGURE 2: PSCAM spectra of (A) the AADH−azurin complex and (B) the MADH−amicyanin complex [difference spectra (oxidized − ascorbate-reduced)]. Thick and thin lines represent spectra recorded along the two principal optical directions lying on the crystal face perpendicular to the incident beam. (C) PSCAM spectra of the AADH−azurin complex before (thin line) and after (thick line) treatment with benzylamine. Both spectra were recorded along the same optical direction.

reduction of TTQ had occurred (Figure 2A). Identical treatment of a crystal of the MADH−amicyanin binary complex gave very similar results (Figure 2B). Furthermore, spectra of AADH−azurin crystals treated with benzylamine exhibited bands characteristic of both the aminoquinol (330 nm) and the semiquinone (425 nm) forms of TTQ (Figure 2C), indicating that a fraction of electrons had been transferred to a one-electron acceptor as shown in eq 1.

$$\mathrm{TTQ(ox)Cu^{2+}} + \mathrm{substrate} \rightarrow \mathrm{TTQ(red)Cu^{2+}} \leftrightarrow \mathrm{TTQ(semi)Cu^{+}} \quad (1)$$

The isolation of the TTQ semiquinone is a characteristic feature of the crystalline state, where stoichiometries of the redox centers are fixed and an equilibrium distribution of the two substrate-derived electrons between them is rapidly achieved. These PSCAM results provided convincing evidence that crystals of an intermolecular complex of AADH and azurin had been obtained. Furthermore, they indicate that the proteins in the crystalline state are competent for catalysis and interprotein electron transfer.

Attempts to determine the AADH−azurin complex structure by molecular replacement using as a search model the structure of MADH from *P. denitrificans*, which is approximately 30% identical in sequence with AADH, were unsuccessful. A search for heavy atom derivatives for use in the multiple-isomorphous replacement method of phase determination was also unsuccessful. Subsequently, data from crystal form 2 were collected at the peak and the remote low-energy regime of the copper fluorescence spectrum for MAD phasing, but only one copper site could be identified, which was insufficient for determining phases. Data from crystal form 3 were also collected at the peak of the copper anomalous signal but were not useful for phasing. However, subsequent use of the newly determined structure of AADH itself, at 1.2 Å resolution (*12*), permitted all three crystal forms of the AADH−azurin complex to be determined by molecular replacement.

Stoichiometry and Crystal Packing of the Complexes. Crystal form 1 contains two AADH $\alpha_2\beta_2$ heterotetramers in the asymmetric unit, but only one bound azurin molecule. Examination of the crystal packing indicates that only one of the four potential azurin binding sites on AADH is accessible, the other three sites being blocked because of crystal contacts. This low stoichiometry of azurin binding in crystal form 1 explains the difficulty encountered in verifying the presence of azurin in this crystal form. Crystal form 2 contains one AADH $\alpha_2\beta_2$ heterotetramer in the asymmetric unit, but again only one azurin molecule is bound to it. Examination of its crystal packing shows also that only one binding site for azurin is accessible in this crystal form. However, in crystal form 3, which also contains one AADH $\alpha_2\beta_2$ heterotetramer in the asymmetric unit, both azurin binding sites are occupied. In crystal form 1, the bound azurin makes slight contact with nearby molecules related by crystallographic symmetry. In crystal forms 2 and 3, the bound azurin molecules make no such contacts with symmetry-related molecules. When all four independent heterotrimers of an AADH $\alpha\beta$ heterodimer in complex with an azurin molecule in the three crystal forms are compared, the geometry of binding of azurin to AADH is identical.

Structural Results. The first structure to be determined corresponded to crystal form 2, which was the best of the three forms and which diffracted to 1.95 Å resolution. Although the electron density of the AADH portion of the structure was very strong and readily interpretable, the corresponding electron density for the azurin portion was weak except where it was in close contact with the AADH portion of the complex (Figure 3). The average temperature factor for the AADH portion of the molecule is 20.3 Å^2, while for the azurin portion, it is 63.5 Å^2 (Figure 4). The *B*-factor plot for the azurin portion of the molecule has a distinct quasi-periodic pattern that correlates well with the secondary structure of azurin and the manner in which azurin interacts with AADH. In the AADH−azurin complex, the azurin is oriented so that the end of the cylindrical molecule containing the turns of the polypeptide chain connecting the odd to even β-strands (i.e., the turns connecting strands 1 and 2, 3 and 4, 5 and 6, and 7 and 8, at the so-called "north end"), where the copper binding site is located (Figure 1A), lies close to AADH. Likewise, the end of the molecule containing the turns connecting even to odd strands (turns 2−3, 4−5, and 6−7, Figure 1A), as well as the N-and

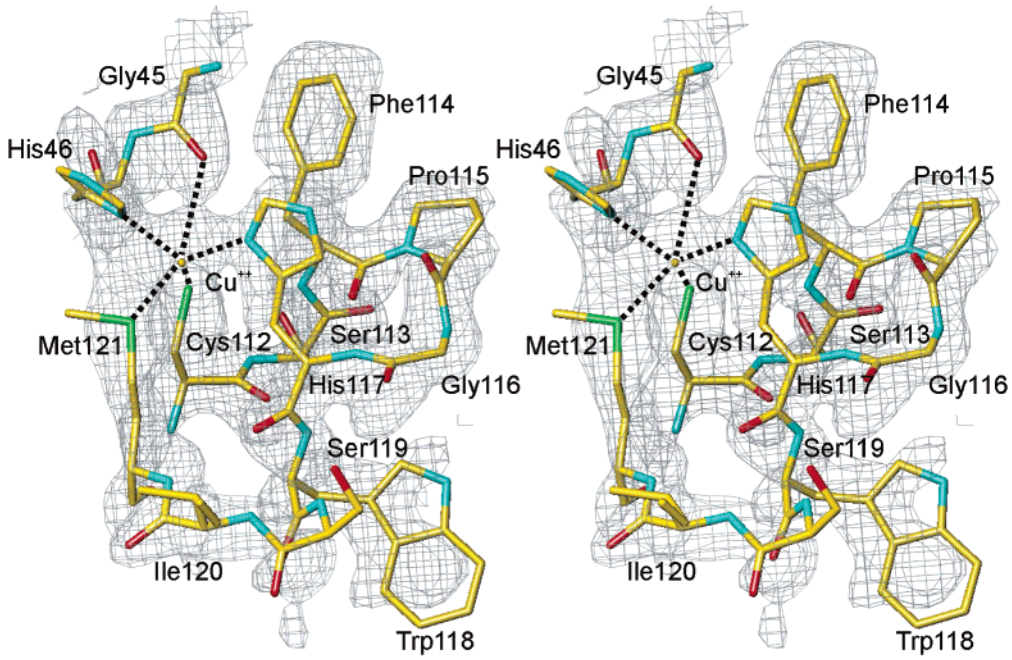

FIGURE 3: Portion of the azurin molecule in crystal from 2 superimposed on the final $2F_o - F_c$ electron density map. The map is contoured at the 1σ level. The portion of the molecule shown includes the copper ion, the copper ligands Gly45 and His46, and the ligand loop from Cys112 to Met121. This figure was prepared using Turbo-Frodo (*31*).

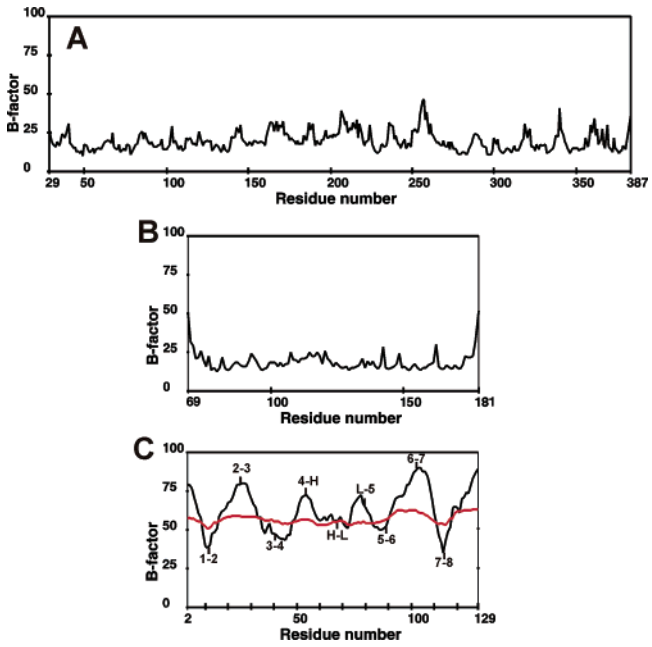

FIGURE 4: *B*-Factor plots of the AADH−azurin complex from crystal form 2. The black lines represent the average of the full atomic isotropic *B*-factors for each residue after the final refinement cycle using CNS: (A) α-subunit of AADH ranging from αPro29 to αVal387, (B) β-subunit of AADH ranging from βGlu69 to βLys181, and (C) γ-subunit (azurin) ranging from Ala2 to Ser129. The labels in the γ-subunit diagram indicate the approximate positions of the turns connecting contiguous strands as shown in Figure 1A. The labels 4-H, H-L, and L-5 denote the turn between strand 4 and the α-helix, the helix−loop turn, and the loop−strand 5 turn as shown in Figure 1A, respectively. The red line represents the average residual isotropic *B*-factor for each residue after subtraction of the contribution from the TLS parameters.

C-termini on strands 1 and 8, is located far from the AADH surface. Those residues in the odd to even category have *B*-factors ranging from 40 to 50 Å^2, while those in the even to odd category have *B*-factors ranging from 80 to 90 Å^2. The helix−strand segment located between β-strands 4 and 5 of azurin follows a similar pattern (Figure 4).

Crystal form 3, in which the azurin is bound to both AADH $\alpha\beta$ heterodimers, is less well ordered than crystal form 2 and diffracts to only 2.5 Å resolution. The average *B*-factors for the AADH and azurin components are 28.6 and 62.0 Å^2, respectively. The pattern of the distribution of *B*-factors along the sequence of azurin is virtually the same for both bound azurin molecules and crystal form 2. Crystal form 1 is also more poorly ordered than crystal form 2. The average *B*-factor for the AADH molecule is 24.6 Å^2 and for the bound azurin molecule is 68.6 Å^2. The *B*-factor distribution for the form 1 azurin molecule is qualitatively similar to that of form 2 but less distinct, and the molecule is less well ordered close to the AADH molecular surface.

To confirm that the observed periodicity in the *B*-factor plot for azurin in crystal form 2 could be explained by anisotropic rigid body motion, two cycles of refinement using 20 TLS parameters (*34*) for each of the five polypeptide chains were carried out using REFMAC. After refinement, the residual *B*-factor plot (after the rigid body motion had been subtracted) for azurin (Figure 4C, red line) was relatively featureless, with an average value of ~55 Å^2. The residual *B*-factor plots for the other subunits were virtually unchanged from the CNS results.

Structure of the Molecule. AADH is a heterotetramer comprising an $(\alpha\beta)_2$ dimer of dimers. The α-subunit is a seven-bladed β-propeller centered on a 7-fold axis of pseudosymmetry. Each "blade" is a four-stranded, twisted antiparallel β-sheet in which the strands progress from the innermost strand close to the central axis outward to the outermost strand and then connects to the innermost strand of the next blade in sequence. There is one disulfide bridge in the α-subunit.

Table 2: Nature of AADH−Azurin and MADH−Amicyanin Interfaces

	AADH−azurin		MADH−amicyanin	
	AADH	azurin	MADH	amicyanin
Δsurface area (Å^2)[a]	−554	−558	−710	−770
no. of residues	17	17	24	19
α-subunit (%)	53	-	38	-
β-subunit (%)	47	-	62	-
hydrophobic residues (%)	74	66	58	65
neutral hydrophilic residues (%)	6	19	14	16
charged residues (%)[b]	19	15	28	15

[a] Change in surface area of each molecule upon complex formation. [b] Includes a buried Asp−Arg salt bridge pair in AADH and MADH.

The β-subunit consists of five β-strands that form two antiparallel β-sheets connected by irregular loops. It contains seven disulfide bridges as well as the TTQ cofactor that consists of tryptophylquinone (Trq), a modified tryptophan side chain at position β109, and an unmodified tryptophan (βTrp160) that are cross-linked through their indole rings. In the αβ dimer, the TTQ is situated at the dimer interface and is sequestered from solvent, although βTrp160 lies close to the protein surface.

AADH−Azurin Interface. Since the azurin is bound to AADH identically in all four complexes observed in the three crystal forms, the model from crystal form 2, which diffracts to the highest resolution (1.95 Å), is used in the following discussions. The AADH−azurin interface covers approximately 550 Å^2 of surface area on each molecule (Table 2). The residues of azurin within the interface, i.e., that exhibit significant lowering of their solvent accessible surface area within the complex, are contained within four segments, residues 11−14, 39−44, 114−120, and 61−72. These are located in the loops between β-strands 1 and 2, β-strands 3 and 4, and β-strands 7 and 8 and at the end of the α-helix and the start of the following loop, respectively (Figure 1). The residues of AADH within the interface include parts of three turns within β-propeller blades 3 and 4 (the turns linking strands 2 and 3 of blade 3, strands 4 and 1 connecting blades 3 and 4, and strands 2 and 3 of blade 4) of the α-subunit and several short segments of the β-subunit surrounding βTrp160 of TTQ. Approximately half of the 17 residues of AADH contained within the interface are on each subunit, and ∼75% of them are hydrophobic (Table 2). Approximately two-thirds of the 17 azurin residues in the interface are hydrophobic. There is one direct hydrogen bond linking AADH and azurin, between βPro106 O of AADH and γSer12 O$^\gamma$ of azurin. The interface contains several water molecules, but none directly link AADH to azurin; one pair of waters bridges the two molecules, linking αPro158 O of AADH and Pro115 O of azurin.

Comparison of the AADH−Azurin Complex with the MADH−Amicyanin Complex. The AADH and MADH α/β heterodimer subunits align with each other with a rmsd of 1.65 Å for 505 equivalent Cα atoms. These residues are 32% identical in sequence. One significant difference between them is the positions of the side chains of βPhe152 and βPhe153 of AADH that replace βPro100 and βGlu101 of MADH (Figure 5). In MADH, these latter surface residues are directed away from βTrp108 of the TTQ redox cofactor, which has a solvent accessible surface area of 13 Å^2. In AADH, the two phenylalanine side chains are directed toward the corresponding residue βTrp160 of the TTQ cofactor and completely block the accessibility of βTrp160 to solvent.

When the three subunits of the MADH−amicyanin complex are aligned with those of the AADH−azurin complex, the MADH and AADH portions of the complexes are aligned quite closely. The amicyanin molecule is also located in the same place as the azurin molecule with respect to the quinoprotein, but its orientation is quite different, being rotated by approximately 90° with respect to azurin (Figure 6A). Despite the large difference in orientations of the copper proteins in the two complexes, the relative positions of the copper atoms in the two complexes are only 4.7 Å apart, and each is positioned as close as possible to the TTQ cofactor in its respective complex.

Comparison of the interfaces of the AADH and MADH complexes shows that the size of the MADH interface is ∼1.5 times larger than that of AADH (Table 2). MADH contains 24 residues within the interface compared to 17 in AADH, and they are localized to the β-subunit to a greater extent. The fraction of hydrophobic residues in the MADH−amicyanin interface is smaller than that in the AADH−azurin interface, and the fraction of neutral hydrophilic and charged residues in the MADH interface is correspondingly larger. However, the number and distribution of hydrophobic and charged residues in amicyanin and azurin are approximately the same in the two complexes.

The connections between the MADH and amicyanin also differ from those between AADH and azurin (Figure 6B). MADH and amicyanin are joined by two salt bridges, one strong and one weak, and by three water molecules that bridge the interface (*7*). AADH is joined to azurin by one hydrogen bond and by two intervening water molecules hydrogen bonded together, but by no individual water molecules. These interfaces are consistent with the results of previous solution studies which showed that the MADH−amicyanin complex was stabilized at low ionic strengths (*19*) while the AADH−azurin complex was stabilized at high ionic strengths (*14*).

Redox Cofactor Separation and Electron Transfer. The distance to the copper ion of azurin from O6 of TTQ in AADH, where substrate oxidation occurs, is 21.0 Å; the shortest distance from βTrp160, the unmodified tryptophan of TTQ (atom Cη2), to the copper is 12.6 Å. The shortest distance from βTrp160 Cη2 to His117 of azurin, the nearest ligand to copper, is 8.7 Å. In the MADH−amicyanin complex, these distances are 16.8, 9.3, and 5.7 Å, respectively. The comparison of these inter-cofactor distances shows that they are ∼3.5 Å longer in the AADH−azurin complex than in the MADH−amicyanin complex. The reason for this is that βTrp160 of AADH is shielded from solvent by the side chains of βPhe152 and βPhe153. The presence of these two side chains in the interface, particularly βPhe153, pushes azurin away from AADH, compared to the MADH−amicyanin interaction, leading to the longer electron transfer distance. As can be seen in Table 3, for each complex there is strong correlation between the experimentally determined values for electron transfer distance and the shortest distance from the unmodified tryptophan of TTQ to the copper as seen in each structure.

A Pathways analysis (*36*) of the AADH−azurin complex was performed to determine the most efficient predicted

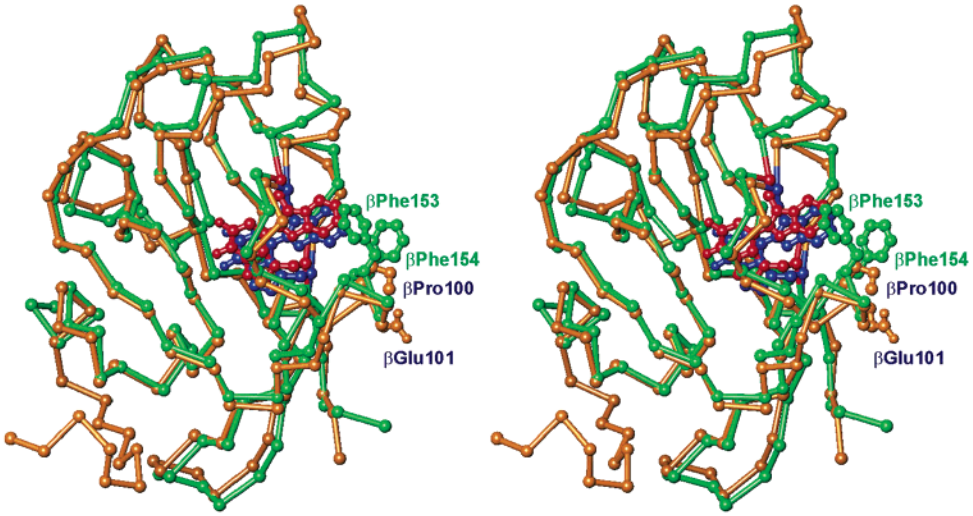

FIGURE 5: Stereo Cα diagram of the superposition of the β-subunits of AADH (green) and MADH (gold). The TTQ of AADH (red) and MADH (blue) are shown as ball-and-stick diagrams. The side chains of βPhe152 and βPhe153 of AADH, which block the access of solvent to βTrp160 of AADH and βPro100 and βPro101 of MADH, that permit the access of solvent to βTrp108 of MADH are drawn as ball-and-stick diagrams. This figure was prepared using Turbo-Frodo (*31*).

pathway for electron transfer from TTQ to copper. For the purpose of this analysis, the electron transfer donor was defined as the entire TTQ cofactor so that the pathway would begin at the most advantageous position on TTQ. The best predicted pathway is shown in Figure 7 and compared with the analogous predicted pathway from the MADH−amicyanin complex. The pathways are very similar but with two key differences. In the MADH−amicyanin complex, the electron is transferred directly from the exposed edge of TTQ to amicyanin. In the AADH−azurin complex, TTQ is not surface exposed and the electron is transferred to azurin via βPhe153. In the MADH−amicyanin complex, the electron enters amicyanin at the backbone O of Pro94 and then tunnels through the His95 ligand to copper. In the AADH−azurin complex, the electron is transferred directly to the His117 ligand. This pathway coupling is the relative efficiency of all possible ET pathways according to eq 2

$$H_{AB} \propto \Pi\epsilon_i \qquad (2)$$

where i ranges over the pathway steps and ϵ_i is a wavefunction decay factor for each step in the pathway. The values assigned for ϵ are 0.6 for transfer through a covalent bond, $0.36e^{-1.7(r-2.8)}$ for transfer through a hydrogen bond, and $0.6e^{-1.7(r-1.4)}$ for a through-space jump (*37*). In each case, the pathway represents the most direct route between redox centers and sets of pathways via the amino acid residues shown in Figure 7 are significantly more favored than any alternative pathways. The structural basis for the difference in coupling is the fact that the presence of βPhe153 prevents direct interaction of amicyanin with the edge of TTQ. The two through-space jumps in the AADH−azurin pathway are each longer than the single through-space jump in the MADH−amicyanin pathway, and this contributes to the approximately 50-fold weaker relative coupling value for the AADH−azurin electron transfer pathway (Table 3). These relative coupling values determined from the structures of each complex correlate very well with the relative values of H_{AB} that were experimentally determined for the true electron transfer reactions of each complex.

DISCUSSION

The composition of the crystals of the putative complex between the two redox partners, AADH and azurin, was uncertain at first and required further analysis for verification of the presence of both component molecules in the crystals. The lack of a distinct blue color in the crystals, the presence of only two bands from SDS−PAGE analysis, and the weakness of the copper signal in the X-ray fluorescence spectrum of the crystals were cause for concern. However, PSCAM measurements of these initial crystals, and subsequent X-ray fluorescence measurements with a new crystal form, confirmed the presence of azurin in the crystals, as well as the reactivity of the proteins in the crystalline state. The low and variable stoichiometry of the azurin binding in two of the three crystal forms added to the difficulty in the initial steps in confirming the presence of the copper-containing component.

Two of the distinctive properties of the AADH−azurin complex that are explained by the crystal structure analysis are the weak nature of the interactions between the components of the complex and the increased stability of the complex that is found with an increased ionic strength. The smaller interface area and fewer links between AADH and azurin compared to those in the MADH−amicyanin complex are consistent with the higher K_m value for the steady state reaction and higher K_d value for transfer of electrons from TTQ to copper in transient kinetic studies (*14*). The large *B*-factors for azurin, especially farther from the interface, are consistent with its weak binding to AADH and suggest that azurin may undergo a rocking motion when bound to AADH. Another ramification of the weak binding of azurin to AADH is manifest in the low stoichiometry of azurin binding in crystal forms 1 and 2 where crystal packing forces allow crystals to form even if some azurin binding sites are blocked by neighboring molecules. If the azurin binding were stronger, it is possible that inclusion of azurin in the absent sites would prevent these crystals from growing. The similarity of the AADH−azurin complex in the four observed binding sites indicates that the interaction among them is very specific, even if it is weaker than in the MADH−

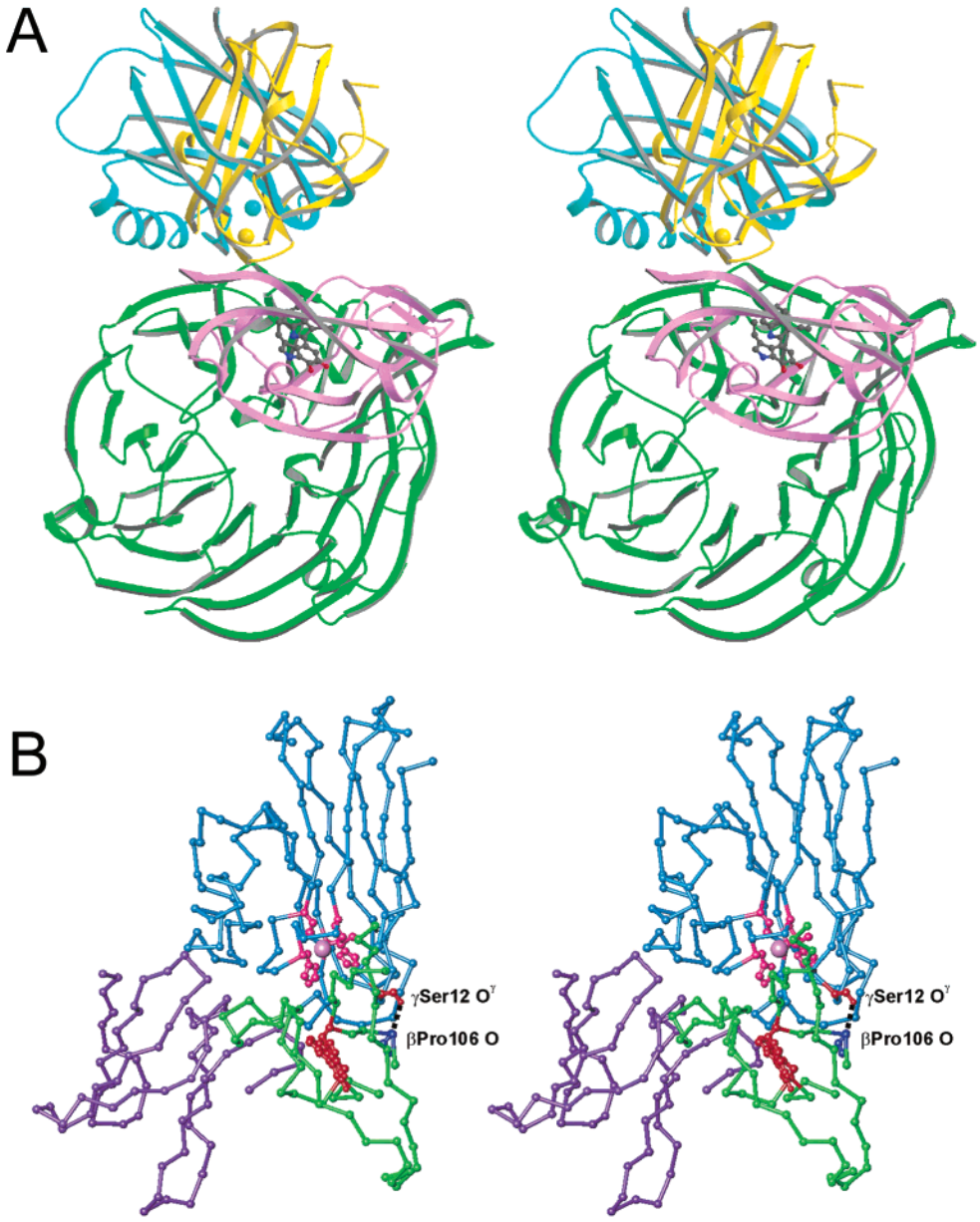

FIGURE 6: Structural diagrams of the AADH−azurin complex. (A) Ribbon diagram of the AADH−azurin complex (green for the α-subunit, magenta for the *β*-subunit, and cyan for azurin) with the amicyanin molecule (gold) superimposed, based on an alignment of the MADH heterodimer of the MADH−amicyanin complex with the heterodimer of AADH. The coppers of azurin and amicyanin are shown as cyan and gold spheres, respectively, and the TTQ is shown as a ball-and-stick diagram (gray for carbon, blue for nitrogen, and red for oxygen). This diagram was prepared using Molscript (*39*) and Raster3D (*40*). (B) Close-up stereoview of the interface between the AADH α-subunit (residues α155−α221, violet) and *β*-subunit (residues *β*105−*β*164, green) with azurin (full molecule, cyan). The four side chain ligands to copper in azurin and the TTQ cofactor of AADH are shown as red ball-and-stick diagrams. The two residues that are hydrogen bonded together (indicated as a dashed line) in the complex, *β*Pro106 (blue) and *γ*Ser12 (red), are also shown as ball-and-stick diagrams. This figure was prepared using Turbo-Frodo (*31*).

amicyanin complex. The kinetic dissociation constants, K_M and K_d, of the AADH−azurin complex are considerably larger that those of the MADH−amicyanin complex. They also react differently to changes in ionic strength, increasing with an increase in ionic strength in the case of the MADH−amicyanin complex and decreasing in the case of the AADH−azurin complex. The greater stabilization of the AADH−azurin complex with an increased ionic strength may be explained by the greater hydrophobic content of the interface when compared to that of the MADH−amicyanin complex.

Another aspect of the AADH−azurin complex is the comparison between kinetics of electron transfer with respect to the MADH−amicyanin complex. Each exhibits a different mechanism of electron transfer depending on whether the dehydrogenase is first reduced by substrate or dithionite. Reduction by substrate yields an aminoquinol form of the reduced cofactor (*38*, *39*). Transfer of electrons to the copper protein requires deprotonation of the aminoquinol which activates the system for very rapid electron transfer which is gated (i.e., rate-limited) by the deprotonation step (*40*). Therefore, the redox reactions of the substrate-reduced enzymes cannot be analyzed by electron transfer theory. In contrast, reduction of TTQ by dithionite yields a quinol form of the reduced cofactor, and transfer of electrons from it to the copper protein is a true electron transfer reaction that

Table 3: Electron Transfer Parameters for the Reactions of Azurin with AADH and of Amicyanin with MADH[a]

	AADH−azurin[b]	MADH−amicyanin[b]
k_{ET} at 30 °C (s^{-1})	5	12
$\Delta G°$ (kJ/mol)	−10.1	−3.2
λ (eV)[c]	1.6 ± 0.1	2.3 ± 0.1
λ (kJ/mol)[c]	154 ± 10	222 ± 10
H_{AB} (cm^{-1})	0.13 ± 0.02	12 ± 7
r calculated for $\beta = 1.0$[d] (Å)	15.2	9.5
r from structure (Å)	12.7	9.4
best pathway coupling (unitless)[e]	6.9×10^{-6}	2.4×10^{-4}

[a] The TTQ of AADH and MADH is in the hydroquinol form in each enzyme and is produced by reduction of the enzyme with dithionite. [b] The electron transfer parameters were obtained from ref *15* for AADH and from ref *42* for MADH. [c] λ is sometimes expressed in units of kilojoules per mole and sometimes as electronvolts so both values are given. [d] Calculated from data in ref *42* using the generally accepted β value for protein β-sheets (*43*) of 1.0 $Å^{-1}$. [e] From this study.

may be analyzed by electron transfer theory (eqs 3 and 4) (*41*).

$$k_{ET} = \frac{4\pi^2 H_{AB}^{\ 2}}{h\sqrt{4\pi\lambda RT}} e^{(-\Delta G°+\lambda)^2/4\lambda RT} \quad (3)$$

$$k_{ET} = k_o \exp[-\beta(r - r_o)] \exp[-(\Delta G° + \lambda)^2/(4\lambda RT)] \quad (4)$$

where λ is the reorganization energy, H_{AB} is the electronic coupling matrix element, h is Planck's constant, T is the temperature, R is the gas constant, and k_o is the characteristic frequency of the nuclei (10^{13} s^{-1}), which is the maximum electron transfer rate when the donor and acceptor are in van der Waals contact and $\lambda = -\Delta G°$. The donor to acceptor distance is r, and r_o is the close contact distance (3 Å). The parameter β is used to quantitate the nature of the intervening medium with respect to its efficiency to mediate ET. $\Delta G°$ is determined from the change in the midpoint potential for the reaction. These true electron transfer reactions for the two systems are compared in the context of the structures which are now available for both complexes.

Examination of the structures reveals that the separations between the TTQ and copper atoms in the two complexes differ by ~3−3.5 Å, with the greater separation observed in the AADH−azurin complex that can be attributed to the replacement of both βPro100 and βGlu101 of MADH with phenylalanine in AADH. These latter side chains shield the tryptophan side chain of TTQ and lead to the observed increases in the copper−TTQ distance which weakens the pathway coupling for the best electron transfer. These differences in electron transfer distance and pathway are reflected in differences in the experimentally determined H_{AB} values in the case of the hydroquinol which have been obtained by analysis of the temperature dependence of the electron transfer rates by eq 2. The much smaller H_{AB} value for electron transfer in the AADH−azurin complex relative to that in the MADH−amicyanin complex correlates well with the weakened pathway coupling calculated from the structures. Despite the differences in coupling, the actual electron transfer rates are similar. This is because the decrease in H_{AB} is offset by a slightly more negative $\Delta G°$ and a much smaller λ for the AADH−azurin reaction (Table 3).

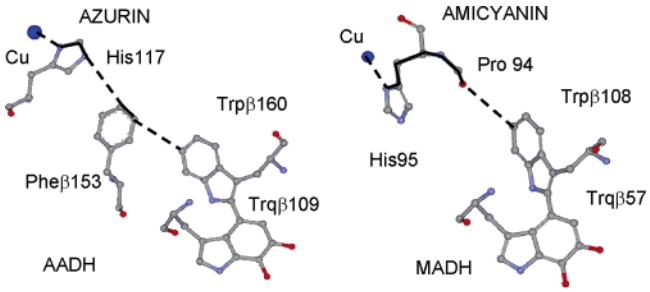

FIGURE 7: Best predicted pathways for transfer of electrons from reduced TTQ to the oxidized copper in the AADH−azurin complex (left) and the MADH−amicyanin complex (right). The reduced electron equivalents are assumed to be delocalized over the entire TTQ ring system. These pathways were calculated using HARLEM (*35*).

Concluding Remarks. The smaller interface area and fewer links between AADH and azurin compared to those in the MADH−amicyanin complex help explain the higher K_m for the complex. Also, the greater hydrophobic content of the AADH−azurin interface may be responsible for the increased stability of the complex at high ionic strengths, a relationship that is the opposite of that observed in the MADH−amicyanin complex. The large *B*-factors for the atoms of azurin, especially farther from the interface, are consistent with weak binding and suggest that azurin may undergo a rocking motion when bound to AADH as confirmed by TLS refinement. The similarity of the AADH−azurin complex in the four observed binding sites indicates that the interaction is very specific, even if less stable than that in the MADH−amicyanin complex. The interference in binding of azurin to AADH observed in four of the eight possible sites by crystal packing forces indicates that the binding energy is relatively weak and is comparable to the lattice forces. The replacement of βPro100 and βGlu101 of MADH with phenylalanine in AADH appears to shield the tryptophan side chain of TTQ, increases the copper−TTQ distance, and weakens the pathway coupling. The relative differences in the structures of the AADH−azurin and MADH−amicyanin complexes correlate well with results of solution studies of the electron transfer reactions between the respective proteins.

ACKNOWLEDGMENT

We thank Dr. Daved Fremont for helpful advice during synchrotron data collection. We also thank Drs. Nigel Scrutton and David Leys for providing us with the AADH coordinates prior to publication. Use of the Advanced Photon Source was supported by the U.S. Department of Energy, Office of Science, Office of Basic Energy Sciences, under Contract W-31-109-ENG-38. We also thank the staff at the SBC and the NE-CAT of the APS for their assistance and use of equipment. The NE-CAT facility at the APS is supported by Grant RR-15301 from the National Center for Research Resources of the National Institutes of Health.

REFERENCES

1. Pelletier, H., and Kraut, J. (1992) Crystal structure of a complex between electron transfer partners, cytochrome c peroxidase and cytochrome c, *Science 258*, 1748−1755.
2. Lange, C., and Hunte, C. (2002) Crystal structure of the yeast cytochrome bc1 complex with its bound substrate cytochrome c, *Proc. Natl. Acad. Sci. U.S.A. 99*, 2800−2805.

3. Toogood, H. S., van Thiel, A., Basran, J., Sutcliffe, M. J., Scrutton, N. S., and Leys, D. (2004) Extensive domain motion and electron transfer in the human electron transferring flavoprotein. Medium chain acyl-CoA dehydrogenase complex, *J. Biol. Chem. 279*, 32904−32912.
4. Leys, D., Basran, J., Talfournier, F., Sutcliffe, M. J., and Scrutton, N. S. (2003) Extensive conformational sampling in a ternary electron transfer complex, *Nat. Struct. Biol. 10*, 219−225.
5. Kurisu, G., Kusunoki, M., Katoh, E., Yamazaki, T., Teshima, K., Onda, Y., Kimata-Ariga, Y., and Hase, T. (2001) Structure of the electron transfer complex between ferredoxin and ferredoxin-$NADP^+$ reductase, *Nat. Struct. Biol. 8*, 117−121.
6. Chen, L., Durley, R., Poliks, B. J., Hamada, K., Chen, Z., Mathews, F. S., Davidson, V. L., Satow, Y., Huizinga, E., and Vellieux, F. M. (1992) Crystal structure of an electron-transfer complex between methylamine dehydrogenase and amicyanin, *Biochemistry 31*, 4959−4964.
7. Chen, L., Durley, R. C., Mathews, F. S., and Davidson, V. L. (1994) Structure of an electron transfer complex: Methylamine dehydrogenase, amicyanin, and cytochrome c_{551i}, *Science 264*, 86−90.
8. Govindaraj, S., Eisenstein, E., Jones, L. H., Sanders-Loehr, J., Chistoserdov, A. Y., Davidson, V. L., and Edwards, S. L. (1994) Aromatic amine dehydrogenase, a second tryptophan tryptophylquinone enzyme, *J. Bacteriol. 176*, 2922−2929.
9. Hyun, Y. L., and Davidson, V. L. (1995) Mechanistic studies of aromatic amine dehydrogenase, a tryptophan tryptophylquinone enzyme, *Biochemistry 34*, 816−823.
10. McIntire, W. S., Wemmer, D. E., Chistoserdov, A., and Lidstrom, M. E. (1991) A new cofactor in a prokaryotic enzyme: Tryptophan tryptophylquinone as the redox prosthetic group in methylamine dehydrogenase, *Science 252*, 817−824.
11. Hyun, Y. L., and Davidson, V. L. (1995) Unusually large isotope effect for the reaction of aromatic amine dehydrogenase. A common feature of quinoproteins? *Biochim. Biophys. Acta 1251*, 198−200.
12. Masgrau, L., Roujeinikova, A., Johannissen, L. O., Hothi, P., Basran, J., Ranaghan, K. E., Mulholland, A. J., Sutcliffe, M. J., Scrutton, N. S., and Leys, D. (2006) Atomic description of an enzyme reaction dominated by proton tunneling, *Science 312*, 237−241.
13. Edwards, S. L., Davidson, V. L., Hyun, Y. L., and Wingfield, P. T. (1995) Spectroscopic evidence for a common electron transfer pathway for two tryptophan tryptophylquinone enzymes, *J. Biol. Chem. 270*, 4293−4298.
14. Hyun, Y. L., and Davidson, V. L. (1995) Electron transfer reactions between aromatic amine dehydrogenase and azurin, *Biochemistry 34*, 12249−12254.
15. Hyun, Y. L., Zhu, Z., and Davidson, V. L. (1999) Gated and ungated electron transfer reactions from aromatic amine dehydrogenase to azurin, *J. Biol. Chem. 274*, 29081−29086.
16. Davidson, V. L. (2002) Chemically gated electron transfer. A means of accelerating and regulating rates of biological electron transfer, *Biochemistry 41*, 14633−14636.
17. Chistoserdov, A. Y. (2001) Cloning, sequencing and mutagenesis of the genes for aromatic amine dehydrogenase from *Alcaligenes faecalis* and evolution of amine dehydrogenases, *Microbiology 147*, 2195−2202.
18. Brooks, H. B., Jones, L. H., and Davidson, V. L. (1993) Deuterium kinetic isotope effect and stopped-flow kinetic studies of the quinoprotein methylamine dehydrogenase, *Biochemistry 32*, 2725−2729.
19. Davidson, V. L., Graichen, M. E., and Jones, L. H. (1993) Binding constants for a physiologic electron-transfer protein complex between methylamine dehydrogenase and amicyanin. Effects of ionic strength and bound copper on binding, *Biochim. Biophys. Acta 1144*, 39−45.
20. Davidson, V. L., Jones, L. H., Graichen, M. E., Mathews, F. S., and Hosler, J. P. (1997) Factors which stabilize the methylamine dehydrogenase-amicyanin electron transfer protein complex revealed by site-directed mutagenesis, *Biochemistry 36*, 12733−12738.
21. Baker, E. N. (1988) Structure of azurin from *Alcaligenes denitrificans* refinement at 1.8 Å resolution and comparison of the two crystallographically independent molecules, *J. Mol. Biol. 203*, 1071−1095.
22. Durley, R., Chen, L., Lim, L. W., Mathews, F. S., and Davidson, V. L. (1993) Crystal structure analysis of amicyanin and apoamicyanin from *Paracoccus denitrificans* at 2.0 Å and 1.8 Å resolution, *Protein Sci. 2*, 739−752.
23. Merli, A., Brodersen, D. E., Morini, B., Chen, Z., Durley, R. C., Mathews, F. S., Davidson, V. L., and Rossi, G. L. (1996) Enzymatic and electron transfer activities in crystalline protein complexes, *J. Biol. Chem. 271*, 9177−9180.
24. Ferrari, D., Merli, A., Peracchi, A., Di V.alentin, M., Carbonera, D., and Rossi, G. L. (2003) Catalysis and electron transfer in protein crystals: The binary and ternary complexes of methylamine dehydrogenase with electron acceptors, *Biochim. Biophys. Acta 1647*, 337−342.
25. McPherson, A. (1999) *Crystallization of biological macromolecules*, Cold Spring Harbor Laboratory Press, Plainview, NY.
26. Otwinowski, Z., and Minor, W. (1997) Processing of X-ray diffraction data collected by oscillation methods, *Methods Enzymol. 276*, 307−326.
27. Chen, L., Mathews, F. S., Davidson, V. L., Tegoni, M., Rivetti, C., and Rossi, G. L. (1993) Preliminary crystal structure studies of a ternary electron transfer complex between a quinoprotein, a blue copper protein, and a c-type cytochrome, *Protein Sci. 2*, 147−154.
28. Rivetti, C., Mozzarelli, A., Rossi, G. L., Henry, E. R., and Eaton, W. A. (1993) Oxygen binding by single crystals of hemoglobin, *Biochemistry 32*, 2888−2906.
29. Pearson, A. R., Mozzarelli, A., and Rossi, G. L. (2004) Microspectrophotometry for structural enzymology, *Curr. Opin. Struct. Biol. 14*, 656−662.
30. Collaborative Computational Project Number 4 (1994) Collaborative computational project number 4, *Acta Crystallogr. D50*, 760−763.
31. Brünger, A. T., Adams, P. D., Clore, G. M., DeLano, W. L., Gros, P., Grosse-Kunstleve, R. W., Jiang, J. S., Kuszewski, J., Nilges, M., Pannu, N. S., Read, R. J., Rice, L. M., Simonson, T., and Warren, G. L. (1998) Crystallography & NMR system: A new software suite for macromolecular structure determination, *Acta Crystallogr. D54*, 905−921.
32. Roussel, A., and Cambillau, C. (1991) in *Silicon graphics geometry partners directory 86*, Silicon Graphics, Mountain View, CA.
33. Schomaker, V., and Trueblood, K. (1968) On the rigid-body motion of molecules in crystals, *Acta Crystallogr. B24*, 63−76.
34. Winn, M. D., Isupov, M. N., and Murshudov, G. N. (2001) Use of tls parameters to model anisotropic displacements in macromolecular refinement, *Acta Crystallogr. D57*, 122−133.
35. Kurnikov, I. V. (2000) *HARLEM*, University of Pittsburgh, Pittsburgh, PA.
36. Onuchic, J. N., Beratan, D. N., Winkler, J. R., and Gray, H. B. (1992) Pathway analysis of protein electron-transfer reactions, *Annu. Rev. Biophys. Biomol. Struct. 21*, 349−377.
37. Regan, J. J., Risser, S. M., Beratan, D. N., and Onuchic, J. N. (1993) Protein electron transport: Single versus multiple pathways, *J. Phys. Chem. 97*, 13083−13088.
38. Bishop, G. R., Valente, E. J., Whitehead, T. L., Brown, K. L., Hicks, R. T., and Davidson, V. L. (1996) Direct detection by ^{15}N-NMR of the tryptophan tryptophylquinone aminoquinol reaction intermediate of methylamine dehydrogenase, *J. Am. Chem. Soc. 118*, 12868−12869.
39. Bishop, G. R., Zhu, Z., Whitehead, T. L., Hicks, R. P., and Davidson, V. L. (1998) Identification of reaction products and intermediates of aromatic-amine dehydrogenase by ^{15}N and ^{13}C NMR, *Biochem. J. 330* (Part 3), 1159−1163.
40. Bishop, G. R., and Davidson, V. L. (1995) Intermolecular electron transfer from substrate-reduced methylamine dehydrogenase to amicyanin is linked to proton transfer, *Biochemistry 34*, 12082−12086.
41. Marcus, R. A., and Sutin, N. (1985) Electron transfers in chemistry and biology, *Biochim. Biophys. Acta 811*, 265−322.
42. Brooks, H. B., and Davidson, V. L. (1994) Kinetic and thermodynamic analysis of a physiologic intermolecular electron-transfer reaction between methylamine dehydrogenase and amicyanin, *Biochemistry 33*, 5696−5701.
43. Gray, H. B., and Winkler, J. R. (2005) Long-range electron transfer, *Proc. Natl. Acad. Sci. U.S.A. 102*, 3534−3539.

BI0612972